Periodic/Aperiodic Motion Control Using Periodic/Aperiodic Separation Filter

Hisayoshi Muramatsu, *Student Member, IEEE*, and Seiichiro Katsura, *Member, IEEE*

***Abstract*—Motion control is a fundamental technique used in automated mechanical systems. Classically, velocity, force, and impedance are controlled in motion control systems, but simultaneous control is difficult. This article proposes periodic/aperiodic (P/A) motion control based on periodicity and aperiodicity of motion. The P/A motion control separately applies different control methods to P/A motions using P/A velocity and P/A force, which are extracted using a periodic/aperiodic separation filter (PASF) from velocity and force. Accordingly, six types of P/A motion controls are constructed in this article, which correspond to different combinations of the P/A velocity, P/A force, and P/A impedance controls. To construct the P/A motion control systems, acceleration control based on a disturbance observer is used. The ACS, which rejects disturbances, enables the P/A motion control design to ignore disturbances. The experiments were conducted to validate the six P/A motion controls, which simultaneously realized two P/A motion control objectives.**

***Index Terms*—Disturbance observer (DOB), force control, impedance control, motion control, periodicity, position control.**

I. Introduction

MECHATRONICS and robotics systems have been widely used in industrial and human support applications. Because the majority of requirements of these systems are related to their physical functioning, motion controls have been studied [1]–[6]. Motion control studies typically focus on one or some motion characteristics, such as position, velocity, acceleration, or force. Furthermore, one degree-of-control-freedom can inherently achieve a single motion control objective, where the degree-of-control-freedom is the number of controllable actuators or axes in this article. For example, velocity control, which does not consider force, risks breaking environments owing to unlimited force in a contact situation. Conversely, velocity of force control is indefinite. These examples indicate the tradeoff between the velocity and force controls. An intermediate control method, that is not as extreme as either the velocity or force controls, is impedance control [7]–[10]. The impedance control can change the impedance parameters of a controlled system: mass, viscosity, and stiffness. However, it also conflicts with the velocity and force controls. Although multiple degrees-of-control-freedom are required to realize multiple control objectives, the number of degrees-of-control-freedom of a mechanical system is limited. Therefore, an outstanding issue related to motion control is achievement for multiple control objectives with a limited number of degrees-of-control-freedom.

Hybrid controls achieve multiple control objectives using multiple degrees-of-control-freedom, in which different controls are assigned to different axes [11]–[14]. Bilateral control, which uses a two degrees-of-control-freedom system based on a master-slave paradigm, enables simultaneous realization of two control objectives: zero-difference of the position and zero-sum of the force between the master and slave systems [15]–[18]. Thus, the hybrid and bilateral controls require additional degrees-of-control-freedom for realizing additional objectives. Optimal control is a standard approach to adjustment of such inconsistent objectives with restrictions. However, it balances conflicting objectives and does not allow simultaneous achievement of both objectives [19], [20]. Another approach is the use of consistent trajectories for the velocity and force [21], where the position trajectory is calculated from the required force reference. In this case, the position cannot be arbitrarily determined.

The aim of this article is to realize two periodic/aperiodic (P/A) motion control objectives simultaneously. Accordingly, the P/A motion control using P/A velocity and P/A force is proposed. A periodic/aperiodic separation filter (PASF) [22] separates velocity and force into the P/A velocity and P/A force, respectively. The separation of objectives and motion into P/A objectives and P/A motions, respectively, enables the simultaneous realization of two control objectives. Conventionally, control approaches that consider periodicity have been studied, such as repetitive control [23]–[27], periodic disturbance observer (DOB) [28], and periodic systems [29]–[31]. However, these methods focus only on the periodicity. Moreover, although the previous study [22] proposed the PASF and P/A state feedback control, it is impractical because disturbance compensation and practical simultaneous control are not addressed. In this article, six types of practical P/A motion controls, that correspond to different combinations of the P/A velocity, P/A force, and P/A impedance controls, are constructed. The six P/A motion controls use acceleration control based on a DOB, which compensates for disturbances [32], [33]. The experiments validated

Manuscript received January 10, 2019; revised May 6, 2019 and July 15, 2019; accepted August 29, 2019. Date of publication October 3, 2019; date of current version April 30, 2020. This work was supported by JSPS KAKENHI under Grant 18H03784 and Grant 19J11506. *(Corresponding author: Seiichiro Katsura.)*

The authors are with the Department of System Design Engineering, Keio University, Yokohama 223-8522, Japan (e-mail: muramatsu@katsura.sd.keio.ac.jp; katsura@sd.keio.ac.jp).

Color versions of one or more of the figures in this article are available online at http://ieeexplore.ieee.org.

Digital Object Identifier 10.1109/TIE.2019.2942535

the practicality of the simultaneous control of P/A velocity, P/A force, and P/A impedance. The novelty, contribution, and significance of this article are as follows.

1) This article utilizes periodicity and aperiodicity for motion control and controls P/A motions separately. This is a new perspective in the motion control field.
2) The proposed P/A motion control enables simultaneous realization of two control objectives assigned to P/A motions with one degree-of-control-freedom.
3) The simultaneous realization of two P/A motion control objectives facilitates appropriate design of motion controllers for diverse situations. For example, a rigid repetitive robot task and soft impedance interaction with sudden human contact can be simultaneously realized.

Moreover, the proposed method can double the number of realizable control objectives of a multidegree-of-control-freedom system, such as a multiaxis manipulator. For example, a three-link-manipulator using the P/A motion control can achieve six P/A motion control objectives for the x, y, and z axes.

II. Periodic/Aperiodic Separation Filter

A. P/A Signal Definitions

In this article, a signal $x(t)$ is assumed to consist of a periodic signal $x_{\mathrm{p}}(t)$ and an aperiodic signal $x_{\mathrm{a}}(t)$ as

$$x(t) = x_{\mathrm{p}}(t) + x_{\mathrm{a}}(t).$$

where $_{\mathrm{p}}$ and $_{\mathrm{a}}$ denote periodic and aperiodic variables, respectively. To define the P/A signals, we rewrite the signal $x(t)$ using the lifting technique as

$$x_\tau(k) = x(k\Pi + \tau),\ k = 0, 1, 2, \ldots \tag{1}$$

where Π is the period of the periodic signal. The parameter k is the discrete time for the lifted signal $x_\tau(k)$ using the period Π as the sampling time. Fig. 1 shows a conceptual diagram of the lifting technique. Since a perfect periodic signal is defined by $x_{\mathrm{p}}(t+\Pi) = x_{\mathrm{p}}(t)$, the corresponding lifted perfect periodic signal is given by

$$x_{\tau\mathrm{p}}(k+1) = x_{\tau\mathrm{p}}(k) \tag{2}$$

which is constant as $x_{\tau\mathrm{p}}(0) = x_{\tau\mathrm{p}}(1) = x_{\tau\mathrm{p}}(2) = x_{\tau\mathrm{p}}(3) = \cdots$. Hence, the lifted periodic signal $x_{\tau\mathrm{p}}(k)$ is defined as the low-frequency elements of the lifted signal $x_\tau(k)$ on the basis of the constant lifted perfect periodic signal. Furthermore, the lifted aperiodic signal $x_{\tau\mathrm{a}}(k)$ is defined as the high-frequency elements of the lifted signal $x_\tau(k)$. It should be noted that the periodic signal $x_{\mathrm{p}}(k)$ and aperiodic signal $x_{\mathrm{a}}(k)$ are not the low- and high-frequency elements. Fig. 1 illustrates a difference and relation between the periodic signal $x_{\mathrm{p}}(k)$, aperiodic signal $x_{\mathrm{a}}(k)$, lifted periodic signal $x_{\tau\mathrm{p}}(k)$, and lifted aperiodic signal $x_{\tau\mathrm{a}}(k)$. The frequency, which divides the lifted signal $x_\tau(k)$ into the lifted periodic signal $x_{\tau\mathrm{p}}(k)$ and lifted aperiodic signal $x_{\tau\mathrm{a}}(k)$, is defined as the separation frequency ρ. The period Π is determined by a period of target periodic motion, such as a repetitive robot task or periodic human operation. If the period is not provided beforehand, adaptive filters and controls that can estimate the period of a periodic signal are helpful [28], [34]–[38].

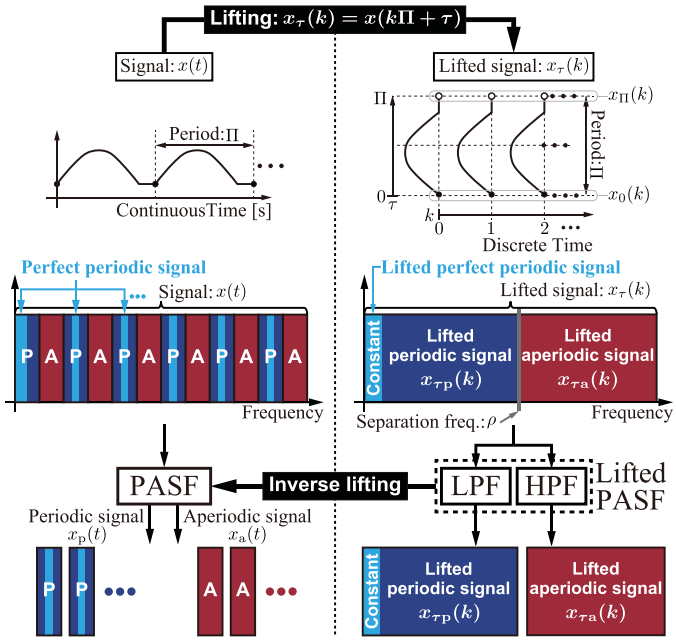

Fig. 1. Conceptual diagram of the derivation of the PASF using the lifting technique.

B. First-Order PASF

A design example of a first-order PASF is described here. It is constructed on the basis of the definitions of the P/A signals. A low-pass filter is used to separate the lifted signal $x_\tau(k)$ into the lifted periodic signal $x_{\tau\mathrm{p}}(k)$ and lifted aperiodic signal $x_{\tau\mathrm{a}}(k)$, which are low- and high-frequency elements, respectively. Consider the first-order low-pass filter

$$LPF(s) = \frac{\rho}{s+\rho} \tag{3}$$

in which the cutoff frequency is the separation frequency ρ. To separate the discrete-time lifted signal $x_\tau(k)$, which is transformed by the lifting technique in (1) from the continuous-time signal $x(t)$, the continuous-time first-order low-pass filter in (3) is Z-transformed using the bilinear transform

$$s = \frac{2}{\Pi}\frac{1-z^{-1}}{1+z^{-1}}$$

into the first-order lifted PASF

$$LPF(z^{-1}) = \frac{\rho\Pi(1+z^{-1})}{\rho\Pi(1+z^{-1}) + 2(1-z^{-1})}. \tag{4}$$

It should be noted that the Z-transformation is based on the period Π of the periodic signal because the sampling time of the discrete-time lifted signal $x_\tau(k)$ is the period Π of the periodic signal. Since the first-order lifted PASF $LPF(z^{-1})$ corresponds to the discrete-time lifted signal $x_\tau(k)$, the first-order PASF $F(s)$ for the continuous-time signal $x(t)$ is calculated by

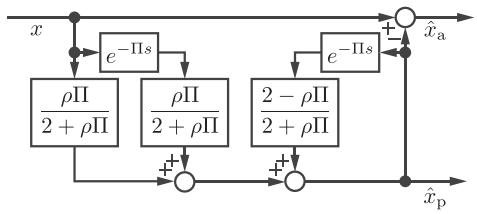

Fig. 2. First-order PASF.

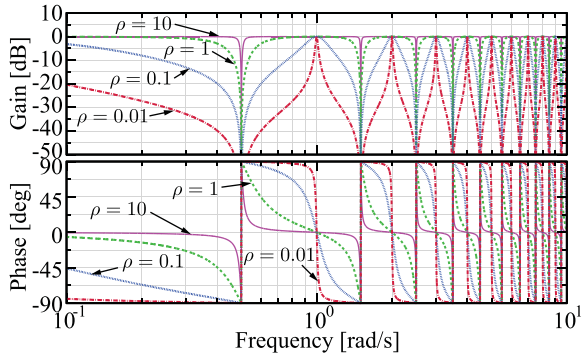

Fig. 3. Bode diagrams of the first-order PASF in (5) with variations in ρ; the period is $\Pi = 2\pi$ s.

substituting $e^{-\Pi s}$ for z^{-1} as

$$F(s) = \frac{\rho\Pi(1+e^{-\Pi s})}{\rho\Pi(1+e^{-\Pi s}) + 2(1-e^{-\Pi s})}. \tag{5}$$

Fig. 1 illustrates the difference between the lifted PASF in (4) and PASF in (5). The first-order PASF provides an estimated periodic signal $\hat{x}_\mathrm{p}(s)$ and estimated aperiodic signal $\hat{x}_\mathrm{a}(s)$ with $F(s)$ as

$$\begin{bmatrix} \hat{x}_\mathrm{p}(s) \\ \hat{x}_\mathrm{a}(s) \end{bmatrix} = \begin{bmatrix} F(s) \\ 1-F(s) \end{bmatrix} x(s) = \boldsymbol{S}(s)x(s). \tag{6}$$

where $\hat{}$ denotes an estimated variable. A block diagram of the first-order PASF is shown in Fig. 2. Bode diagrams of the first-order PASF in (5) are shown in Fig. 3, with variations in the separation frequency ρ. The Bode diagrams show differences of the PASF from a band-pass filter. As a perfect periodic signal expressed by the Fourier series expansion is $x_\mathrm{p}(t) = \frac{a_0}{2} + \sum_{n=1}^{\infty}[a_n \cos(n\omega_0 t) + b_n \sin(n\omega_0 t)]$, a separation filter for the P/A signals needs to be able to extract the constant element $\frac{a_0}{2}$ and an infinite number of waves $\sum_{n=1}^{\infty}[a_n \cos(n\omega_0 t) + b_n \sin(n\omega_0 t)]$. ω_0 denotes the fundamental frequency. The PASF can extract all of the elements of the perfect periodic signal, as shown in Fig. 3, because the gain is 0 dB at the frequencies $n\omega_0,\ n = 0, 1, 2, \ldots$, unlike a band-pass filter which can only extract a sinusoidal wave. Moreover, the phase of the PASF for the perfect periodic signal at the frequencies $n\omega_0,\ n = 0, 1, 2, \ldots$ is 0 deg.

C. Separation Frequency

A separation example using the first-order PASF is shown in Fig. 4. The original signal includes the pseudoimpulse signals at 6 and 21 s and white noise for 11–13 and 26–28 s. The first-order PASF separates the original signal into the P/A signals using the two separation frequencies: $\rho = 1$ and $\rho = 0.01$. $\rho = 0.01$ realizes a more proper separation for extracting the inputted P/A signals compared with $\rho = 1$. This is because a low separation frequency defines a periodic signal close to the perfect periodic signal. In contrast, a high separation frequency defines a periodic signal close to the original signal. Thus, the separation frequency ρ adjusts the balance between the periodic signal $x_\mathrm{p}(t)$ and aperiodic signal $x_\mathrm{a}(t)$ in the signal $x(t)$.

The time constant of the PASF also depends on the separation frequency. The time constant of the first-order PASF is $1/\rho$ calculated from the low-pass filter in (3). Fig. 5 shows convergence examples of the first-order PASF for different separation frequencies ρ and verifies the time constant. This indicates that a high separation frequency causes fast convergence of the first-order PASF.

Consequently, the separation frequency should be determined from the tradeoff between the proper separation (low separation frequency) and fast convergence (high separation frequency). A requirement T_c for the time constant $1/\rho \leq T_\mathrm{c}$ leads to the inequality for the separation frequency: $1/T_\mathrm{c} \leq \rho$. Since the minimal separation frequency yields the most proper separation, the separation frequency can be determined by

$$\rho = 1/T_\mathrm{c}.$$

Alternatively, two separation frequencies for transient and steady phases can be separately determined, as shown in Fig. 4.

D. Interference Between the Estimated P/A Signals

Practically, interference occurs between the estimated P/A signals. As the lifted periodic signal $x_{\tau\mathrm{p}}(k)$ and lifted aperiodic signal $x_{\tau\mathrm{a}}(k)$ are defined as the low- and high-frequency elements of the lifted signal $x_\tau(k)$, the ideal separation requires an ideal low-pass filter. However, the ideal low-pass filter is unfeasible and the actual lifted PASF in (4) requires use of a proper low-pass filter. Consequently, the unideal actual lifted PASF causes the interference between the estimated P/A signals in practical situations.

The interference appears as an aperiodic signal of the estimated periodic signal and a periodic signal of the estimated aperiodic signal. These are approximately given by

$$\begin{bmatrix} \hat{x}_{\mathrm{pp}}(s) \\ \hat{x}_{\mathrm{pa}}(s) \end{bmatrix} = \boldsymbol{S}(s)\hat{x}_\mathrm{p}(s), \quad \begin{bmatrix} \hat{x}_{\mathrm{ap}}(s) \\ \hat{x}_{\mathrm{aa}}(s) \end{bmatrix} = \boldsymbol{S}(s)\hat{x}_\mathrm{a}(s) \tag{7}$$

where $\hat{x}_{\mathrm{pa}}(s)$ and $\hat{x}_{\mathrm{ap}}(s)$ are the interference elements. They are equal because $\hat{x}_{\mathrm{pa}}(s) = [1-F(s)]F(s)x(s)$ and $\hat{x}_{\mathrm{ap}}(s) = F(s)[1-F(s)]x(s)$ from (6). In the separation example shown in Fig. 4, the green line corresponds to the approximate interference elements. This verifies that the interference is not dominant and may be negligible. Although the interference remains, a high-order PASF can reduce the interference.

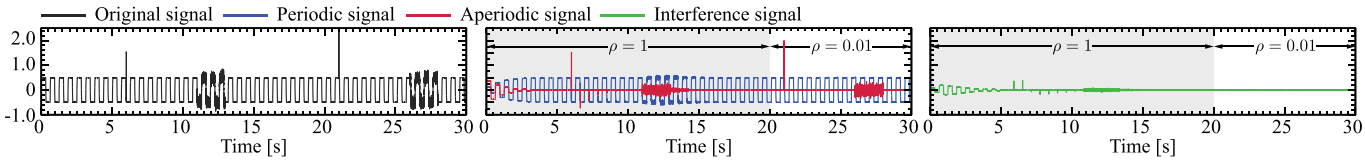

Fig. 4. Separation example of the first-order PASF; the period is $\Pi = 0.2\pi$ s.

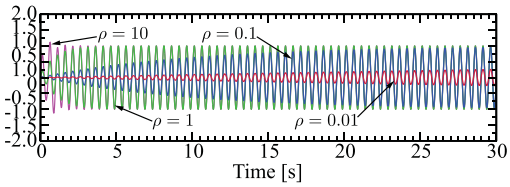

Fig. 5. Convergence of the first-order PASF, for different separation frequencies ρ; the period is $\Pi = 0.5$ s.

III. P/A Motion Control

PVAF control

$$\hat{v}_{\mathrm{p}} = \varphi_{\mathrm{pvaf}}^{-1} F[C_{\mathrm{v}}\left(v_{\mathrm{p}}^{\mathrm{cmd}} + \hat{n}_{\mathrm{vp}}\right) + K_{\mathrm{f}}(f_{\mathrm{a}}^{\mathrm{cmd}} - \hat{f}_{\mathrm{a}}^{\mathrm{exo}} + \hat{n}_{\mathrm{fa}})] \tag{8}$$

$$\hat{f}_{\mathrm{a}} = \varphi_{\mathrm{pvaf}}^{-1}(1-F)Z_{\mathrm{e}}[C_{\mathrm{v}}(v_{\mathrm{p}}^{\mathrm{cmd}} + \hat{n}_{\mathrm{vp}}) + K_{\mathrm{f}}(f_{\mathrm{a}}^{\mathrm{cmd}} - \hat{f}_{\mathrm{a}}^{\mathrm{exo}} + \hat{n}_{\mathrm{fa}})] \tag{9}$$

$$\varphi_{\mathrm{pvaf}}(s) = s + K_{\mathrm{f}}Z_{\mathrm{e}} + (C_{\mathrm{v}} - K_{\mathrm{f}}Z_{\mathrm{e}})F$$

$$\hat{v}_{\mathrm{p}} = \frac{C_{\mathrm{v}}}{s + C_{\mathrm{v}}}(v_{\mathrm{p}}^{\mathrm{cmd}} + \hat{n}_{\mathrm{vp}}) \tag{10}$$

$$\hat{f}_{\mathrm{a}} = \frac{K_{\mathrm{f}}Z_{\mathrm{e}}}{s + K_{\mathrm{f}}Z_{\mathrm{e}}}(f_{\mathrm{a}}^{\mathrm{cmd}} - \hat{f}_{\mathrm{a}}^{\mathrm{exo}} + \hat{n}_{\mathrm{fa}}) \tag{11}$$

$$T_{\mathrm{pvaf}}(s) = -\frac{Qs + K_{\mathrm{f}}Z_{\mathrm{e}} + (C_{\mathrm{v}} - K_{\mathrm{f}}Z_{\mathrm{e}})F}{s + M_{\mathrm{n}}^{-1}(1-Q)Z_{\mathrm{e}} + K_{\mathrm{f}}Z_{\mathrm{e}} + (C_{\mathrm{v}} - K_{\mathrm{f}}Z_{\mathrm{e}})F}. \tag{12}$$

PFAV control

$$\hat{f}_{\mathrm{p}} = \varphi_{\mathrm{pfav}}^{-1} F Z_{\mathrm{e}}[K_{\mathrm{f}}(f_{\mathrm{p}}^{\mathrm{cmd}} - \hat{f}_{\mathrm{p}}^{\mathrm{exo}} + \hat{n}_{\mathrm{fp}}) + C_{\mathrm{v}}(v_{\mathrm{a}}^{\mathrm{cmd}} + \hat{n}_{\mathrm{va}})] \tag{13}$$

$$\hat{v}_{\mathrm{a}} = \varphi_{\mathrm{pfav}}^{-1}(1-F)[K_{\mathrm{f}}(f_{\mathrm{p}}^{\mathrm{cmd}} - \hat{f}_{\mathrm{p}}^{\mathrm{exo}} + \hat{n}_{\mathrm{fp}}) + C_{\mathrm{v}}(v_{\mathrm{a}}^{\mathrm{cmd}} + \hat{n}_{\mathrm{va}})] \tag{14}$$

$$\varphi_{\mathrm{pfav}}(s) = s + C_{\mathrm{v}} + (K_{\mathrm{f}}Z_{\mathrm{e}} - C_{\mathrm{v}})F$$

$$\hat{f}_{\mathrm{p}} = \frac{K_{\mathrm{f}}Z_{\mathrm{e}}}{s + K_{\mathrm{f}}Z_{\mathrm{e}}}(f_{\mathrm{p}}^{\mathrm{cmd}} - \hat{f}_{\mathrm{p}}^{\mathrm{exo}} + \hat{n}_{\mathrm{fp}}) \tag{15}$$

$$\hat{v}_{\mathrm{a}} = \frac{C_{\mathrm{v}}}{s + C_{\mathrm{v}}}(v_{\mathrm{a}}^{\mathrm{cmd}} + \hat{n}_{\mathrm{va}}) \tag{16}$$

$$T_{\mathrm{pfav}}(s) = -\frac{Qs + C_{\mathrm{v}} + (K_{\mathrm{f}}Z_{\mathrm{e}} - C_{\mathrm{v}})F}{s + M_{\mathrm{n}}^{-1}(1-Q)Z_{\mathrm{e}} + C_{\mathrm{v}} + (K_{\mathrm{f}}Z_{\mathrm{e}} - C_{\mathrm{v}})F}. \tag{17}$$

PVAI control

$$\hat{v}_{\mathrm{p}} = \varphi_{\mathrm{pvai}}^{-1} F C_{\mathrm{v}}[H_{\mathrm{v}}(v_{\mathrm{p}}^{\mathrm{cmd}} + v_{\mathrm{a}}^{\mathrm{cmd}} + n_{\mathrm{v}}) - \hat{f}_{\mathrm{a}}^{\mathrm{exo}} + \hat{n}_{\mathrm{fa}}] \tag{18}$$

$$\hat{v}_{\mathrm{a}} = \varphi_{\mathrm{pvai}}^{-1}(1-F)C_{\mathrm{v}}[H_{\mathrm{v}}(v_{\mathrm{p}}^{\mathrm{cmd}} + v_{\mathrm{a}}^{\mathrm{cmd}} + n_{\mathrm{v}}) - \hat{f}_{\mathrm{a}}^{\mathrm{exo}} + \hat{n}_{\mathrm{fa}}] \tag{19}$$

$$\varphi_{\mathrm{pvai}}(s) = (s + C_{\mathrm{v}})H_{\mathrm{v}} + C_{\mathrm{v}}Z_{\mathrm{e}}(1-F)$$

$$\hat{v}_{\mathrm{p}} = \frac{C_{\mathrm{v}}}{s + C_{\mathrm{v}}}(v_{\mathrm{p}}^{\mathrm{cmd}} + \hat{n}_{\mathrm{vp}}) \tag{20}$$

$$\frac{C_{\mathrm{v}}}{s + RC_{\mathrm{v}}}(v_{\mathrm{a}}^{\mathrm{cmd}} + \hat{n}_{\mathrm{va}}) - \hat{v}_{\mathrm{a}} = \frac{C_{\mathrm{v}}}{s + RC_{\mathrm{v}}}\frac{1}{H_{\mathrm{v}}}(\hat{f}_{\mathrm{a}}^{\mathrm{exo}} - \hat{n}_{\mathrm{fa}}) \tag{21}$$

$$T_{\mathrm{pvai}}(s) = -\frac{QH_{\mathrm{v}}s + C_{\mathrm{v}}H_{\mathrm{v}} + C_{\mathrm{v}}Z_{\mathrm{e}}(1-F)}{[s + M_{\mathrm{n}}^{-1}(1-Q)Z_{\mathrm{e}} + C_{\mathrm{v}}]H_{\mathrm{v}} + C_{\mathrm{v}}Z_{\mathrm{e}}(1-F)}. \tag{22}$$

PIAV control

$$\hat{v}_{\mathrm{p}} = \varphi_{\mathrm{piav}}^{-1} F C_{\mathrm{v}}[H_{\mathrm{v}}(v_{\mathrm{p}}^{\mathrm{cmd}} + v_{\mathrm{a}}^{\mathrm{cmd}} + n_{\mathrm{v}}) - \hat{f}_{\mathrm{p}}^{\mathrm{exo}} + \hat{n}_{\mathrm{fp}}] \tag{23}$$

$$\hat{v}_{\mathrm{a}} = \varphi_{\mathrm{piav}}^{-1}(1-F)C_{\mathrm{v}}H_{\mathrm{v}}[H_{\mathrm{v}}(v_{\mathrm{p}}^{\mathrm{cmd}} + v_{\mathrm{a}}^{\mathrm{cmd}} + n_{\mathrm{v}}) - \hat{f}_{\mathrm{p}}^{\mathrm{exo}} + \hat{n}_{\mathrm{fp}}] \tag{24}$$

$$\varphi_{\mathrm{piav}}(s) = (s + C_{\mathrm{v}})H_{\mathrm{v}} + C_{\mathrm{v}}Z_{\mathrm{e}}F$$

$$\frac{C_{\mathrm{v}}}{s + RC_{\mathrm{v}}}(v_{\mathrm{p}}^{\mathrm{cmd}} + \hat{n}_{\mathrm{vp}}) - \hat{v}_{\mathrm{p}} = \frac{C_{\mathrm{v}}}{s + RC_{\mathrm{v}}}\frac{1}{H_{\mathrm{v}}}(\hat{f}_{\mathrm{p}}^{\mathrm{exo}} - \hat{n}_{\mathrm{fp}}) \tag{25}$$

$$\hat{v}_{\mathrm{a}} = \frac{C_{\mathrm{v}}}{s + C_{\mathrm{v}}}(v_{\mathrm{a}}^{\mathrm{cmd}} + \hat{n}_{\mathrm{va}}) \tag{26}$$

$$T_{\mathrm{piav}}(s) = -\frac{QH_{\mathrm{v}}s + C_{\mathrm{v}}H_{\mathrm{v}} + C_{\mathrm{v}}Z_{\mathrm{e}}F}{[s + M_{\mathrm{n}}^{-1}(1-Q)Z_{\mathrm{e}} + C_{\mathrm{v}}]H_{\mathrm{v}} + C_{\mathrm{v}}Z_{\mathrm{e}}F}. \tag{27}$$

PFAI control

$$\hat{f}_{\mathrm{p}} = \varphi_{\mathrm{pfai}}^{-1} F Z_{\mathrm{e}}[f_{\mathrm{p}}^{\mathrm{cmd}} - f^{\mathrm{exo}} + n_{\mathrm{f}} + Z_{\mathrm{v}}(v_{\mathrm{a}}^{\mathrm{cmd}} + \hat{n}_{\mathrm{va}})] \tag{28}$$

$$\hat{v}_{\mathrm{a}} = \varphi_{\mathrm{pfai}}^{-1}(1-F)[f_{\mathrm{p}}^{\mathrm{cmd}} - f^{\mathrm{exo}} + n_{\mathrm{f}} + Z_{\mathrm{v}}(v_{\mathrm{a}}^{\mathrm{cmd}} + \hat{n}_{\mathrm{va}})] \tag{29}$$

$$\varphi_{\mathrm{pfai}}(s) = M_{\mathrm{v}}s + Z_{\mathrm{e}} + Z_{\mathrm{v}}(1-F)$$

$$\hat{f}_{\mathrm{p}} = \frac{Z_{\mathrm{e}}}{M_{\mathrm{v}}s + Z_{\mathrm{e}}}(f_{\mathrm{p}}^{\mathrm{cmd}} - \hat{f}_{\mathrm{p}}^{\mathrm{exo}} + \hat{n}_{\mathrm{fp}}) \tag{30}$$

$$Z_{\mathrm{v}}(v_{\mathrm{a}}^{\mathrm{cmd}} + \hat{n}_{\mathrm{va}}) - RH_{\mathrm{v}}\hat{v}_{\mathrm{a}} = (\hat{f}_{\mathrm{a}}^{\mathrm{exo}} - \hat{n}_{\mathrm{fa}}) \tag{31}$$

$$T_{\mathrm{pfai}}(s) = -\frac{QM_{\mathrm{v}}s + Z_{\mathrm{e}} + Z_{\mathrm{v}}(1-F)}{M_{\mathrm{v}}[s + M_{\mathrm{n}}^{-1}(1-Q)Z_{\mathrm{e}}] + Z_{\mathrm{e}} + Z_{\mathrm{v}}(1-F)}. \tag{32}$$

TABLE I
SIX P/A MOTION CONTROLS

Control type	Control objective for periodic motion	Control objective for aperiodic motion
Periodic velocity and aperiodic force (PVAF) control	$v_{\mathrm{p}}^{\mathrm{cmd}} - \hat{v}_{\mathrm{p}} = 0$	$f_{\mathrm{a}}^{\mathrm{cmd}} - \hat{f}_{\mathrm{a}} = 0$
Periodic force and aperiodic velocity (PFAV) control	$f_{\mathrm{p}}^{\mathrm{cmd}} - \hat{f}_{\mathrm{p}} = 0$	$v_{\mathrm{a}}^{\mathrm{cmd}} - \hat{v}_{\mathrm{a}} = 0$
Periodic velocity and aperiodic impedance (PVAI) control	$v_{\mathrm{p}}^{\mathrm{cmd}} - \hat{v}_{\mathrm{p}} = 0$	$M_{\mathrm{v}}\dot{v}_{\mathrm{a}}^{\mathrm{imp}} + D_{\mathrm{v}}v_{\mathrm{a}}^{\mathrm{imp}} + K_{\mathrm{v}}\int_{t_0}^{t_f} v_{\mathrm{a}}^{\mathrm{imp}}dt = \hat{f}_{\mathrm{a}}$
Periodic impedance and aperiodic velocity (PIAV) control	$M_{\mathrm{v}}\dot{v}_{\mathrm{p}}^{\mathrm{imp}} + D_{\mathrm{v}}v_{\mathrm{p}}^{\mathrm{imp}} + K_{\mathrm{v}}\int_{t_0}^{t_f} v_{\mathrm{p}}^{\mathrm{imp}}dt = \hat{f}_{\mathrm{p}}$	$v_{\mathrm{a}}^{\mathrm{cmd}} - \hat{v}_{\mathrm{a}} = 0$
Periodic force and aperiodic impedance (PFAI) control	$f_{\mathrm{p}}^{\mathrm{cmd}} - \hat{f}_{\mathrm{p}} = 0$	$M_{\mathrm{v}}\dot{v}_{\mathrm{a}}^{\mathrm{imp}} + D_{\mathrm{v}}v_{\mathrm{a}}^{\mathrm{imp}} + K_{\mathrm{v}}\int_{t_0}^{t_f} v_{\mathrm{a}}^{\mathrm{imp}}dt = \hat{f}_{\mathrm{a}}$
Periodic impedance and aperiodic force (PIAF) control	$M_{\mathrm{v}}\dot{v}_{\mathrm{p}}^{\mathrm{imp}} + D_{\mathrm{v}}v_{\mathrm{p}}^{\mathrm{imp}} + K_{\mathrm{v}}\int_{t_0}^{t_f} v_{\mathrm{p}}^{\mathrm{imp}}dt = \hat{f}_{\mathrm{p}}$	$f_{\mathrm{a}}^{\mathrm{cmd}} - \hat{f}_{\mathrm{a}} = 0$

TABLE II
SELECTION MATRICES AND CONTROLLER VECTOR FOR THE SIX P/A MOTION CONTROLS

	Selection FF matrix $\boldsymbol{\Gamma}_{\mathrm{ff}}$	Selection FB matrix $\boldsymbol{\Gamma}_{\mathrm{fb}}$	Controller vector $\boldsymbol{C}$
PVAF	$\boldsymbol{\Gamma}_{\mathrm{ff}} = \begin{bmatrix} 1 & 0 & 0 & 0; & 0 & 0 & 0 & 1 \end{bmatrix}$	$\boldsymbol{\Gamma}_{\mathrm{fb}} = \begin{bmatrix} -1 & 0 & 0 & 0; & 0 & 0 & 0 & -1 \end{bmatrix}$	$\boldsymbol{C} = \begin{bmatrix} K_{\mathrm{i}}/s + K_{\mathrm{d}} & K_{\mathrm{f}} \end{bmatrix}$
PFAV	$\boldsymbol{\Gamma}_{\mathrm{ff}} = \begin{bmatrix} 0 & 0 & 1 & 0; & 0 & 1 & 0 & 0 \end{bmatrix}$	$\boldsymbol{\Gamma}_{\mathrm{fb}} = \begin{bmatrix} 0 & 0 & -1 & 0; & 0 & -1 & 0 & 0 \end{bmatrix}$	$\boldsymbol{C} = \begin{bmatrix} K_{\mathrm{f}} & K_{\mathrm{i}}/s + K_{\mathrm{d}} \end{bmatrix}$
PVAI	$\boldsymbol{\Gamma}_{\mathrm{ff}} = \begin{bmatrix} 1 & 0 & 0 & 0; & 0 & 1 & 0 & 0 \end{bmatrix}$	$\boldsymbol{\Gamma}_{\mathrm{fb}} = \begin{bmatrix} -1 & 0 & 0 & 0; & 0 & -1 & 0 & -H_{\mathrm{v}}^{-1} \end{bmatrix}$	$\boldsymbol{C} = \begin{bmatrix} K_{\mathrm{i}}/s + K_{\mathrm{d}} & K_{\mathrm{i}}/s + K_{\mathrm{d}} \end{bmatrix}$
PIAV	$\boldsymbol{\Gamma}_{\mathrm{ff}} = \begin{bmatrix} 1 & 0 & 0 & 0; & 0 & 1 & 0 & 0 \end{bmatrix}$	$\boldsymbol{\Gamma}_{\mathrm{fb}} = \begin{bmatrix} -1 & 0 & -H_{\mathrm{v}}^{-1} & 0; & 0 & -1 & 0 & 0 \end{bmatrix}$	$\boldsymbol{C} = \begin{bmatrix} K_{\mathrm{i}}/s + K_{\mathrm{d}} & K_{\mathrm{i}}/s + K_{\mathrm{d}} \end{bmatrix}$
PFAI	$\boldsymbol{\Gamma}_{\mathrm{ff}} = \begin{bmatrix} 0 & 0 & 1 & 0; & 0 & Z_{\mathrm{v}} & 0 & 0 \end{bmatrix}$	$\boldsymbol{\Gamma}_{\mathrm{fb}} = \begin{bmatrix} 0 & 0 & -1 & 0; & 0 & -Z_{\mathrm{v}} & 0 & -1 \end{bmatrix}$	$\boldsymbol{C} = \begin{bmatrix} 1/M_{\mathrm{v}} & 1/M_{\mathrm{v}} \end{bmatrix}$
PIAF	$\boldsymbol{\Gamma}_{\mathrm{ff}} = \begin{bmatrix} Z_{\mathrm{v}} & 0 & 0 & 0; & 0 & 0 & 0 & 1 \end{bmatrix}$	$\boldsymbol{\Gamma}_{\mathrm{fb}} = \begin{bmatrix} -Z_{\mathrm{v}} & 0 & -1 & 0; & 0 & 0 & 0 & -1 \end{bmatrix}$	$\boldsymbol{C} = \begin{bmatrix} 1/M_{\mathrm{v}} & 1/M_{\mathrm{v}} \end{bmatrix}$

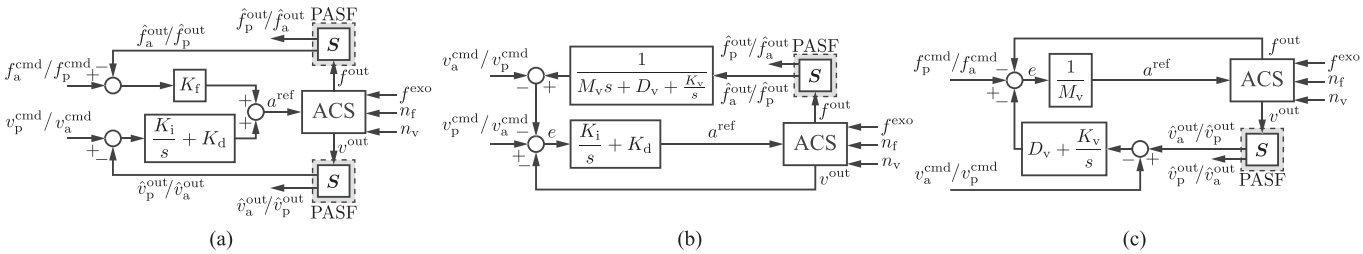

Fig. 6. Block diagrams of the six P/A motion control systems. (a) PVAF/PFAV controls. (b) PVAI/PIAV controls. (c) PFAI/PIAF controls.

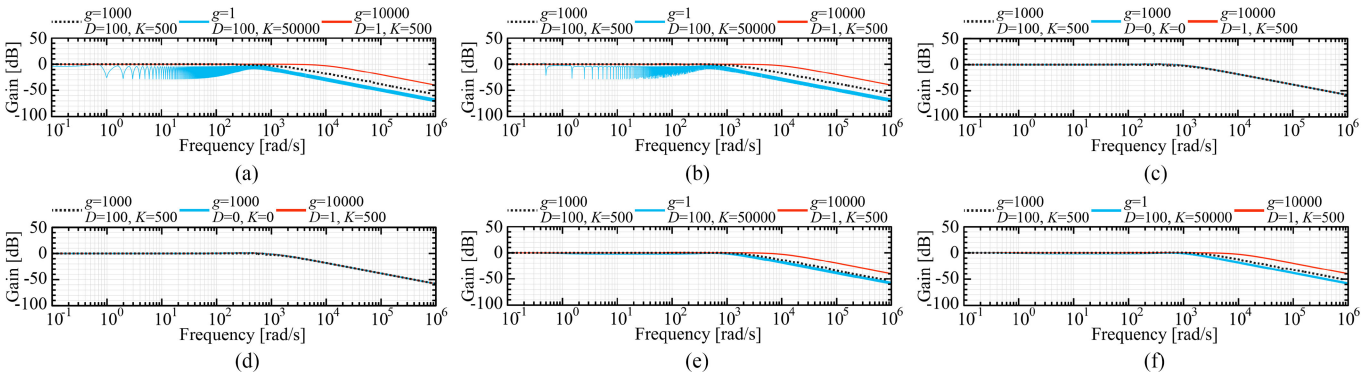

Fig. 7. Bode diagrams of the complementary sensitivity functions of the P/A motion control systems; the parameters are $M_{\mathrm{n}} = 0.3$, $K_{\mathrm{tn}} = 0.24$, $K_{\mathrm{i}} = 6400$, $K_{\mathrm{d}} = 240$, $K_{\mathrm{f}} = 5$, $M_{\mathrm{v}} = 0.1$, $D_{\mathrm{v}} = 50$, $K_{\mathrm{v}} = 800$, $\rho = 1$ rad/s, and $\Pi = 2\pi$ s. (a) PVAF (b) PFAV (c) PVAI (d) PIAV (e) PFAI (f) PIAF.

PIAF control

$$\hat{v}_{\mathrm{p}} = \varphi_{\mathrm{piaf}}^{-1} F[Z_{\mathrm{v}}(v_{\mathrm{p}}^{\mathrm{cmd}} + \hat{n}_{\mathrm{vp}}) + f_{\mathrm{a}}^{\mathrm{cmd}} - f^{\mathrm{exo}} + n_{\mathrm{f}}] \quad (33)$$

$$\hat{f}_{\mathrm{a}} = \varphi_{\mathrm{piaf}}^{-1}(1-F)Z_{\mathrm{e}}[Z_{\mathrm{v}}(v_{\mathrm{p}}^{\mathrm{cmd}} + \hat{n}_{\mathrm{vp}}) + f_{\mathrm{a}}^{\mathrm{cmd}} - f^{\mathrm{exo}} + n_{\mathrm{f}}] \quad (34)$$

$$\varphi_{\mathrm{piaf}}(s) = M_{\mathrm{v}}s + Z_{\mathrm{e}} + Z_{\mathrm{v}}F$$

$$Z_{\mathrm{v}}(v_{\mathrm{p}}^{\mathrm{cmd}} + \hat{n}_{\mathrm{vp}}) - RH_{\mathrm{v}}\hat{v}_{\mathrm{p}} = (\hat{f}_{\mathrm{p}}^{\mathrm{exo}} - \hat{n}_{\mathrm{fp}}) \quad (35)$$

$$\hat{f}_{\mathrm{a}} = \frac{Z_{\mathrm{e}}}{M_{\mathrm{v}}s + Z_{\mathrm{e}}}(f_{\mathrm{a}}^{\mathrm{cmd}} - \hat{f}_{\mathrm{a}}^{\mathrm{exo}} + \hat{n}_{\mathrm{fa}}) \quad (36)$$

$$T_{\mathrm{piaf}}(s) = -\frac{QM_{\mathrm{v}}s + Z_{\mathrm{e}} + Z_{\mathrm{v}}F}{M_{\mathrm{v}}[s + M_{\mathrm{n}}^{-1}(1-Q)Z_{\mathrm{e}}] + Z_{\mathrm{e}} + Z_{\mathrm{v}}F}. \quad (37)$$

TABLE III
EXPERIMENTAL PARAMETERS

Description	Symbol	Position	Force	Impedance	PVAF	PFAV	PVAI	PIAV	PFAI	PIAF
Controlled joint		1st, 2nd, 3rd	1st	2nd, 3rd	1st	1st	1st, 2nd, 3rd	2nd, 3rd	1st	1st
Initial posture from Fig. 8		(b)	(a)	(c)	(a)	(a)	(b)	(c)	(a)	(a)
Sampling time	T_s [ms]	0.1								
Length	L [m]	0.26, 0.27, 0.09								
Gear ratio	G_r	192, 120, 80								
Nominal torque constant	K_{tn} [Nm/A]	0.59, 0.59, 0.238								
Nominal inertia	J_n [Kgm^2]	7.3, 0.86, 0.008	1.28	0.86, 0.008	1.28	1.28	7.3, 0.86, 0.008	0.86, 0.008	1.28	1.28
Period	Π [s]	2								
Separation frequency	ρ [rad/s]	1.0 if $t < 10$ s, 0.01 otherwise								
		Cutoff frequencies [rad/s]								
Pseudo derivative for velocity		1000								
RTOB for torque estimation		100, 100, 100	500	300, 300	500	500	100, 100, 100	300, 300	500	500
DOB		100, 100, 100	500	300, 300	500	500	100, 100, 100	300, 300	500	500
		Control parameters								
Proportional gain	K_i	400, 400, 400	-	400, 400	6400	6400	400, 400, 400	400, 400	-	-
Differential gain	K_d	40, 40, 40	-	40, 40	160	240	40, 40, 40	40, 40	-	-
Proportional gain	K_f	-	2	-	5	2	-	-	3	3
Virtual inertia	J_v [Kgm^2]	-	-	2, 0.1	-	-	3, 2, 0.1	2, 0.1	0.5	0.5
Virtual viscosity	D_v [Nms/rad]	-	-	50, 5	-	-	100, 50, 0.5	50, 5	10	10
Virtual stiffness	K_v [Nm/rad]	-	-	300, 100	-	-	600, 400, 1	300, 100	1000	1000

A. General P/A Motion Control

This article constructs the P/A motion control system using the approximate acceleration control system (ACS)

$$\begin{bmatrix} v \\ f \end{bmatrix} = \begin{bmatrix} 1/s & 0 \\ Z_e/s & 1 \end{bmatrix} \begin{bmatrix} a^{\mathrm{ref}} \\ f^{\mathrm{exo}} \end{bmatrix} \tag{38}$$

$$[v^{\mathrm{out}} \quad f^{\mathrm{out}}]^{\mathrm{T}} = [v \quad f]^{\mathrm{T}} - [n_v \quad n_f]^{\mathrm{T}} \tag{39}$$

where $Z_e(s) = D + K/s$ is the environmental function. v, f, D, K, a^{ref}, f^{exo}, v^{out}, f^{out}, n_v, and n_f denote the velocity response, force response, viscosity, stiffness, acceleration reference, exogenous force, measured velocity, measured force, velocity noise, and force noise, respectively. The ACS is based on the DOB presented in previous studies [32], [33], [39], [40]. In addition, the linearization techniques for nonlinear systems [41], [42] and friction compensation methods [43], [44] are helpful. An ACS based on a classical DOB is demonstrated here for a motor system

$$v = (Ms)^{-1}(K_t I - f),\ f = Z_e v + f^{\mathrm{exo}}$$

where M, K_t, and I denote the mass, thrust constant, and current input, respectively. The current input consisting of the acceleration reference a^{ref} and compensation current I^{cmp} forms the ACS

$$I = K_{tn}^{-1} M_n a^{\mathrm{ref}} + I^{\mathrm{cmp}}$$

where the classical DOB is

$$I^{\mathrm{cmp}} = K_{tn}^{-1} Q(s)[K_{tn} I - M_n s v^{\mathrm{out}}],\ Q(s) = \frac{g}{s+g}$$

where $_n$ and g are a nominal variable and the cutoff frequency, respectively. The sensitivity and complementary sensitivity functions of the ACS are $\frac{s}{s+g}$ and $\frac{g}{s+g}$. Hence, the ACS realizes sufficient disturbance attenuation and robust stability for usual practical applications, and approximately satisfies (38) and (39). If the classical DOB is not sufficient to attenuate disturbances, the ACS can employ another high-order Q-filter.

(a) (b) (c)

Fig. 8. Three initial manipulator postures.

Using the PASF in (6), the general P/A motion controller for the approximate ACS is

$$\begin{bmatrix} \hat{v}_p^{\mathrm{out}} & \hat{v}_a^{\mathrm{out}} & \hat{f}_p^{\mathrm{out}} & \hat{f}_a^{\mathrm{out}} \end{bmatrix}^{\mathrm{T}} = \begin{bmatrix} \boldsymbol{S} & 0 \\ 0 & \boldsymbol{S} \end{bmatrix} \begin{bmatrix} v^{\mathrm{out}} \\ f^{\mathrm{out}} \end{bmatrix}$$

$$a^{\mathrm{ref}} = \boldsymbol{C} \begin{bmatrix} e_p \\ e_a \end{bmatrix},\ \begin{bmatrix} e_p \\ e_a \end{bmatrix} = \boldsymbol{\Gamma}_{\mathrm{fb}} \begin{bmatrix} \hat{v}_p^{\mathrm{out}} \\ \hat{v}_a^{\mathrm{out}} \\ \hat{f}_p^{\mathrm{out}} \\ \hat{f}_a^{\mathrm{out}} \end{bmatrix} + \boldsymbol{\Gamma}_{\mathrm{ff}} \begin{bmatrix} v_p^{\mathrm{cmd}} \\ v_a^{\mathrm{cmd}} \\ f_p^{\mathrm{cmd}} \\ f_a^{\mathrm{cmd}} \end{bmatrix}$$

which generates the acceleration reference a^{ref}. Here, $\boldsymbol{C}$, $\boldsymbol{\Gamma}_{\mathrm{ff}}$, $\boldsymbol{\Gamma}_{\mathrm{fb}}$, e, and $^{\mathrm{cmd}}$ are the controller vector, selection feedforward matrix, selection feedback matrix, error, and a command variable, respectively.

B. Six P/A Motion Controls

Six P/A motion controls, that are combinations of velocity, force, and impedance controls, are designed in this article, and are summarized in Table I, where $v_p^{\mathrm{imp}} = v_p^{\mathrm{cmd}} - \hat{v}_p$ and $v_a^{\mathrm{imp}} = v_a^{\mathrm{cmd}} - \hat{v}_a$. The velocity commands v_p^{cmd} and v_a^{cmd} used for the impedance controls are equilibrium points. Table II gives the selection matrices and controller vector: $\boldsymbol{\Gamma}_{\mathrm{ff}}$, $\boldsymbol{\Gamma}_{\mathrm{fb}}$, and $\boldsymbol{C}$, in which $H_v = M_v s + Z_v$ and $Z_v = D_v + K_v/s$. Additionally,

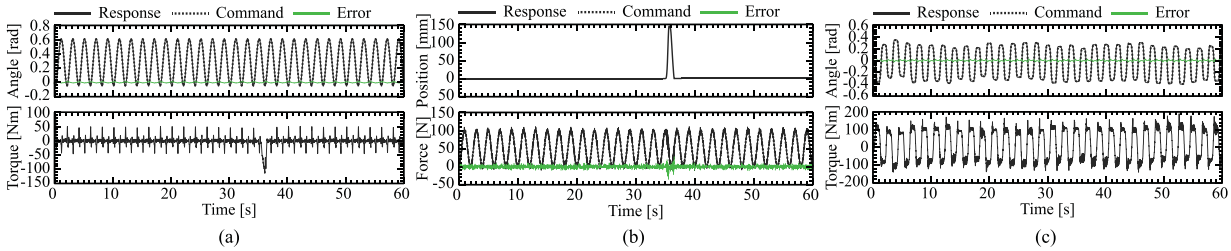

Fig. 9. Experimental results for the position, force, and impedance controls. (a) Position control. (b) Force control. (c) Impedance control.

$M_{\rm v}$, $D_{\rm v}$, and $K_{\rm v}$ are the virtual mass, virtual viscosity, and virtual stiffness, respectively. Block diagrams of the six P/A motion control systems are shown in Fig. 6. Using the approximate ACS in (38) and (39), the nominal input–output transfer functions of the six P/A motion control systems are given by (8), (9), (13), (14), (18), (19), (23), (24), (28), (29), (33), and (34). $C_{\rm v} = K_{\rm i}/s + K_{\rm d}$ is the velocity controller. Moreover, the assumption simplifies the parameter design for the P/A motion controls.

Assumption: The interference is negligible as $\hat{x}_{\rm pa} \approx 0$, $\hat{x}_{\rm ap} \approx 0$, $\hat{x}_{\rm pp} \approx \hat{x}_{\rm p}$, and $\hat{x}_{\rm aa} \approx \hat{x}_{\rm a}$.

The transfer functions then become (10), (11), (15), (16), (20), (21), (25), (26), (30), (31), (35), and (36), where $R = 1 + H_{\rm v}^{-1} Z_{\rm e}$. The transfer functions show the achievement of the control objectives in Table I, and are the same as those of classical velocity, force, and impedance controls. Hence, the gain and impedance parameters: $K_{\rm i}$, $K_{\rm d}$, $K_{\rm f}$, $M_{\rm v}$, $D_{\rm v}$, and $K_{\rm v}$ of the P/A motion controllers can be designed in a similar manner to the classical velocity, force, and impedance controls.

C. Robust Stability

The robust stability guarantees that the P/A motion control is stable under various uncertainties. A modeling error Δ of the motor system is defined by

$$v = (1 + \Delta) K_{\rm tn} (M_{\rm n} s + Z_{\rm e})^{-1} I.$$

The modeling error Δ consists of the weighting function $W(s)$ and variation $\delta(s)$ as $\Delta(s) = W(s)\delta(s)$, where the variation satisfies $\|\delta(s)\|_\infty \leq 1$. The six P/A motion control systems and modeling error are assumed to be nominally stable. The nominal stability of the six P/A motion control systems can be designed and confirmed by poles of the transfer functions: (8), (9), (13), (14), (18), (19), (23), (24), (28), (29), (33), and (34). Then, the robust stability condition based on the small-gain theorem is $\|W(s)T(s)\|_\infty < 1$. $T(s)$ is a complementary sensitivity function, which is an index to evaluate the robust stability. The complementary sensitivity functions of the P/A motion control systems are given by (12), (17), (22), (27), (32), and (37). To satisfy the robust stability condition, the cutoff frequency g of the DOB and parameters for the P/A motion control: $K_{\rm i}$, $K_{\rm d}$, $K_{\rm f}$, $M_{\rm v}$, $D_{\rm v}$, and $K_{\rm v}$ can adjust the complementary sensitivity functions. Fig. 7 shows the Bode diagrams of the complementary sensitivity functions with variations in the environmental parameters: the viscosity D and stiffness K. In practical applications, a complementary sensitivity function usually needs to have a low-pass characteristic to satisfy the robust stability condition because modeling errors typically occur for high frequencies. Thus, the P/A motion control systems are robustly stable owing to the low-pass characteristics.

IV. Experiments

A. Setup

Three experiments were conducted for the conventional methods: position, force, and impedance controls, and six experiments were conducted for the proposed six P/A motion controls. In the experiments, the position control equivalent to the velocity control was used, rather than the velocity control. A six axes manipulator MOTOMAN YR-UPJ3-B00 was used, as shown in Fig. 8. Manipulator angle responses were measured by position encoders and torque responses were estimated by reaction torque observers (RTOBs) [15], [45], [46]. The controlled joints, initial posture, and parameters are summarized in Table III. The separation frequency ρ of the first-order PASF was set to 1.0 if $t < 10$ s for fast convergence, and 0.01 otherwise for proper separation. The controllers were implemented using the real-time application interface for Linux, where the source code for the controllers was written in C++. Each control was implemented with the DOB in the joint space. The experimental control commands were set as follows:

PVAF control

$$v_{\rm p}^{\rm cmd}/s = 50[1 - \cos(\pi t)] \text{ mm}$$
$$f_{\rm a}^{\rm cmd} = \begin{cases} -100 & \text{N} \quad \text{if } 36 < t \leq 38 \\ 0 & \text{N} \quad \text{otherwise} \end{cases}.$$

PFAV control

$$f_{\rm p}^{\rm cmd} = 50[1 - \cos(\pi t)] \text{ N}$$
$$v_{\rm a}^{\rm cmd}/s = \begin{cases} 50\sin\{0.5\pi(t-36)\} & \text{mm} \quad \text{if } 36 < t \leq 38 \\ 0 & \text{mm} \quad \text{otherwise} \end{cases}.$$

PVAI control

$$v_{{\rm p}x}^{\rm cmd}/s = 50[\cos(\pi t) - 1] \text{ mm}, \; v_{{\rm p}y}^{\rm cmd}/s = 50\sin(\pi t) \text{ mm}.$$

PIAV control

$$v_{\rm a}^{\rm cmd}/s = 0 \text{ mm}.$$

PFAI control

$$f_{\rm p}^{\rm cmd} = 50[1 - \cos(\pi t)] \text{ N}.$$

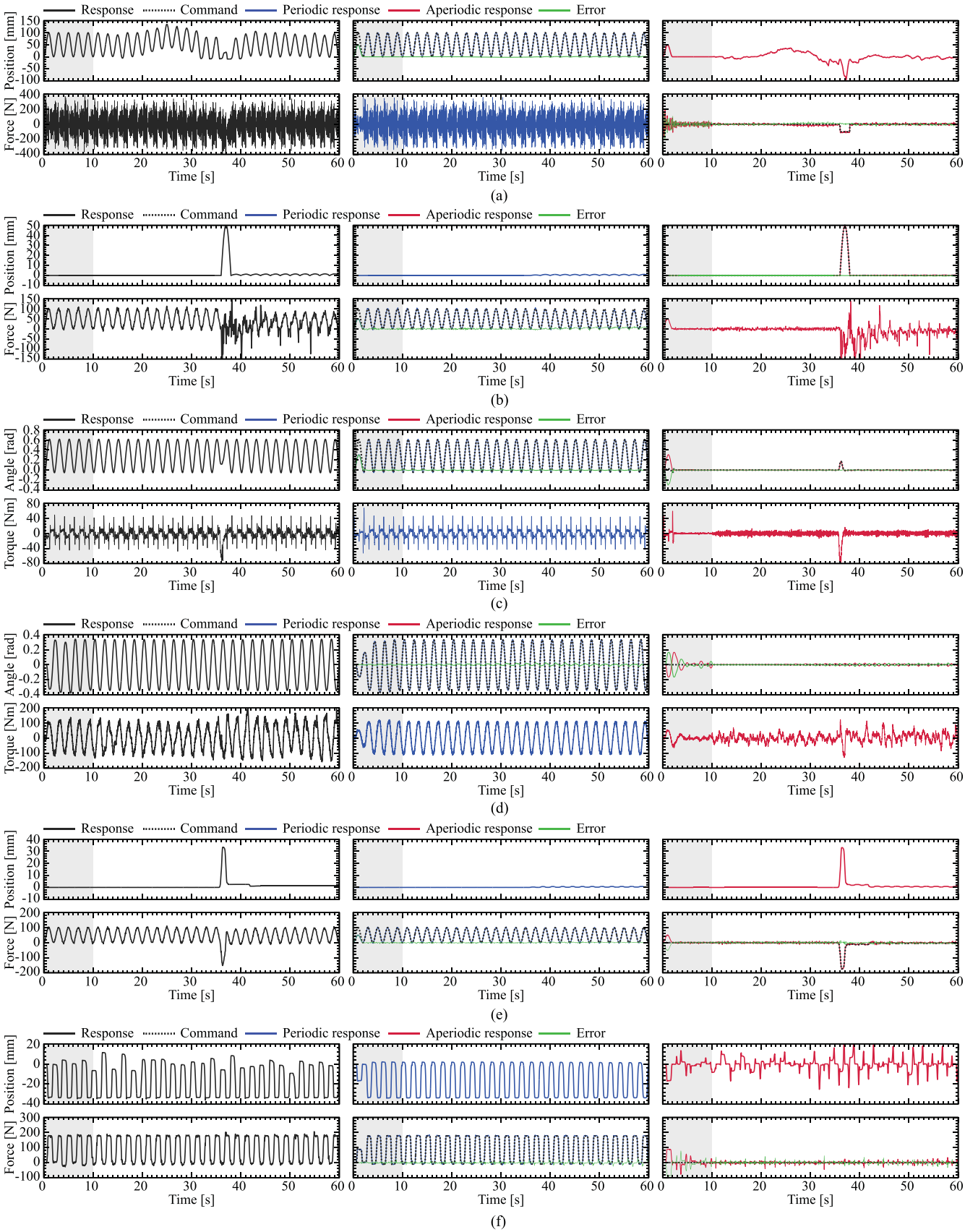

Fig. 10. Experimental results for the six P/A motion controls. (a) PVAF. (b) PFAV. (c) PVAI. (d) PIAV. (e) PFAI. (f) PIAF.

PIAF control

$$f_{\mathrm{a}}^{\mathrm{cmd}} = 0\ \mathrm{N}.$$

In the position, force, PVAI, and PFAI control experiments, an operator contacted the manipulator at approximately 36 s to verify their impedance characteristics. The operator moved the manipulator at all times during the experiments for the impedance, PIAV, and PIAF controls. During the experiments on the six P/A motion controls, the position, force, or impedance control was used if $t < 10$ s for the convergence of the PASF. The PVAF and PVAI controls used the position control, PFAV and PFAI controls used the force control, and PIAV and PIAF controls used the impedance control. The P/A motion controls were applied otherwise.

B. Results

In the graphs of the experimental results, the position or force command signals for the impedance controls were calculated from the force (torque) or position (angle) responses and virtual impedance parameters in Table III. The experimental results for the position, force, and impedance controls are discussed as follows.

1) Position, Force, and Impedance Controls: The position control realized angle command tracking, as shown in Fig. 9(a). The angle response rejected the exogenous torque due to the operator contact at approximately 36 s. However, the torque response was indefinite. Conversely, the force control achieved control of the force response in Fig. 9(b) by rejecting the force variation due to the operator contact at approximately 36 s. Its position response was indefinite and was moved by the contact owing to the control of the force. Fig. 9(c) shows the impedance control between the angle and torque. The small position tracking error implies realization of the impedance control. However, the angle and torque responses could not be arbitrarily controlled.

The focus of the conventional methods was on either the position, force, or impedance. Next, the experimental results for the six P/A motion controls are discussed.

2) PVAF and PFAV Controls: For the PVAF control, the periodic position tracking and aperiodic force tracking were validated, as shown in Fig. 10(a). The PVAF control did not handle the aperiodic force and periodic position as the position and force controls did not control the force and position, respectively. For the PFAV control in Fig. 10(b), the periodic force and aperiodic position were successfully controlled. Accordingly, the PFAV did not control the periodic position and aperiodic force.

3) PVAI and PIAV Controls: Fig. 10(c) and (d) shows the representative experimental results for the second joint of the manipulator. The simultaneous realization of the periodic position and aperiodic impedance controls in Fig. 10(c) and that of the periodic impedance and aperiodic position controls in Fig. 10(d) were validated.

4) PFAI and PIAF Controls: The PFAI control achieved force and impedance controls for periodic and aperiodic motions, respectively, in Fig. 10(e). Additionally, the PIAF control achieved impedance and force controls for periodic and aperiodic motions, respectively, in Fig. 10(e).

The experiments validated the simultaneous realization of two P/A motion control objectives compared with the conventional controls that focused on either the position, force, or impedance. Also, the experiments exhibited a limitation of the P/A motion control that only one of periodic velocity, force, and impedance and only one of aperiodic velocity, force, and impedance can be controlled.

V. Conclusion

This article achieved the simultaneous realization of two P/A motion control objectives with one degree-of-control-freedom. A P/A motion control scheme was proposed by utilizing periodicity and aperiodicity of motion, in which the PASF separated motion into P/A motions. Six types of P/A motion controls were presented: PVAF, PFAV, PVAI, PIAV, PFAI, and PIAF controls, as combinations of the velocity, force, and impedance controls for P/A motions. The input–output transfer functions of the six P/A motion control systems demonstrated that the P/A motion controllers can be designed in a similar manner to the velocity, force, and impedance controls. Moreover, the robust stability was verified with the complementary sensitivity functions of the six P/A motion control systems. The P/A motion control has two limitations. One is that although interference between the estimated P/A signals of the PASF can be negligible, simultaneous realization is not perfectly achieved owing to the interference. The other is that only one of periodic velocity, force, and impedance and only one of aperiodic velocity, force, and impedance can be controlled. The experiments validated the practical performance of the six P/A motion controls.

References

[1] A. Sabanovic and K. Ohnishi, *Motion Control Systems*. Hoboken, NJ, USA: Wiley, 2011.

[2] K. Ohnishi, M. Shibata, and T. Murakami, "Motion control for advanced mechatronics," *IEEE/ASME Trans. Mechatronics*, vol. 1, no. 1, pp. 56–67, Mar. 1996.

[3] M. Makarov, M. Grossard, P. Rodrguez-Ayerbe, and D. Dumur, "Modeling and preview H_∞ control design for motion control of elastic-joint robots with uncertainties," *IEEE Trans. Ind. Electron.*, vol. 63, no. 10, pp. 6429–6438, Oct. 2016.

[4] A. Sabanovic, "Variable structure systems with sliding modes in motion control—A survey," *IEEE Trans. Ind. Electron.*, vol. 7, no. 2, pp. 212–223, May 2011.

[5] D. Xing, F. Liu, S. Liu, and D. Xu, "Motion control for cylindrical objects in microscope's view using a projection method–I: Collision detection and detach control," *IEEE Trans. Ind. Electron.*, vol. 64, no. 7, pp. 5524–5533, Jul. 2017.

[6] L. Sun, M. Cheng, H. Wen, and L. Song, "Motion control and performance evaluation of a magnetic-geared dual-rotor motor in hybrid powertrain," *IEEE Trans. Ind. Electron.*, vol. 64, no. 3, pp. 1863–1872, Mar. 2017.

[7] N. Hogan, "Impedance control: An approach to manipulation: Part I–Theory. Part II–Implementation. Part III–Applications," *J. Dyn. Syst., Meas. Control*, vol. 107, no. 1, pp. 1–24, Mar. 1985.

[8] G. Ferretti, G. Magnani, and P. Rocco, "Impedance control for elastic joints industrial manipulators," *IEEE Trans. Robot. Autom.*, vol. 20, no. 3, pp. 488–498, Jun. 2004.

[9] F. Ficuciello, L. Villani, and B. Siciliano, "Variable impedance control of redundant manipulators for intuitive human–robot physical interaction," *IEEE Trans. Robot.*, vol. 31, no. 4, pp. 850–863, Aug. 2015.

[10] J. Koivumki and J. Mattila, "Stability-guaranteed impedance control of hydraulic robotic manipulators," *IEEE/ASME Trans. Mechatronics*, vol. 22, no. 2, pp. 601–612, Apr. 2017.

[11] M. H. Raibert and J. J. Craig, "Hybrid position/force control of manipulators," *J. Dyn. Syst., Meas. Control*, vol. 103, no. 2, pp. 126–133, Jun. 1981.
[12] F. Jatta, G. Legnani, and A. Visioli, "Friction compensation in hybrid force/velocity control of industrial manipulators," *IEEE Trans. Ind. Electron.*, vol. 53, no. 2, pp. 604–613, Apr. 2006.
[13] S. Sakaino, T. Sato, and K. Ohnishi, "Precise position/force hybrid control with modal mass decoupling and bilateral communication between different structures," *IEEE Trans. Ind. Informat.*, vol. 7, no. 2, pp. 266–276, May 2011.
[14] Y. Nagatsu and S. Katsura, "Decoupling and performance enhancement of hybrid control for motion-copying system," *IEEE Trans. Ind. Electron.*, vol. 64, no. 1, pp. 420–431, Jan. 2017.
[15] C. Mitsantisuk, K. Ohishi, and S. Katsura, "Estimation of action/reaction forces for the bilateral control using Kalman filter," *IEEE Trans. Ind. Electron.*, vol. 59, no. 11, pp. 4383–4393, Nov. 2012.
[16] T. Nozaki, T. Mizoguchi, and K. Ohnishi, "Decoupling strategy for position and force control based on modal space disturbance observer," *IEEE Trans. Ind. Electron.*, vol. 61, no. 2, pp. 1022–1032, Feb. 2014.
[17] M. Takeya, Y. Kawamura, and S. Katsura, "Data reduction design based on delta-sigma modulator in quantized scaling-bilateral control for realizing of haptic broadcasting," *IEEE Trans. Ind. Electron.*, vol. 63, no. 3, pp. 1962–1971, Mar. 2016.
[18] S. Sakaino, T. Furuya, and T. Tsuji, "Bilateral control between electric and hydraulic actuators using linearization of hydraulic actuators," *IEEE Trans. Ind. Electron.*, vol. 64, no. 6, pp. 4631–4641, Jun. 2017.
[19] F. Logist, S. Sager, C. Kirches, and J. F. Van Impe, "Efficient multiple objective optimal control of dynamic systems with integer controls," *J. Process Control*, vol. 20, no. 7, pp. 810–822, Aug. 2010.
[20] A. A. Malikopoulos, "A multiobjective optimization framework for online stochastic optimal control in hybrid electric vehicles," *IEEE Trans. Control Syst. Technol.*, vol. 24, no. 2, pp. 440–450, Mar. 2016.
[21] B. Pandurangan, R. Landers, and S. Balakrishnan, "Hierarchical optimal force-position control of a turning process," *IEEE Trans. Control Syst. Technol.*, vol. 13, no. 2, pp. 321–327, Mar. 2005.
[22] H. Muramatsu and S. Katsura, "Separated periodic/aperiodic state feedback control using periodic/aperiodic separation filter based on lifting," *Automatica*, vol. 101, pp. 458–466, Mar. 2019.
[23] T. Inoue, M. Nakano, T. Kubo, S. Matsumoto, and H. Baba, "High accuracy control of a proton synchrotron magnet power supply," *Proc. IFAC*, vol. 20, pp. 216–221, 1981.
[24] S. Hara, Y. Yamamoto, T. Omata, and M. Nakano, "Repetitive control system: A new type servo system for periodic exogenous signals," *IEEE Trans. Autom. Control*, vol. AC-33, no. 7, pp. 659–668, Jul. 1988.
[25] H. Fujimoto, "RRO compensation of hard disk drives with multirate repetitive perfect tracking control," *IEEE Trans. Ind. Electron.*, vol. 56, no. 10, pp. 3825–3831, Oct. 2009.
[26] R. Sakthivel, S. Mohanapriya, H. R. Karimi, and P. Selvaraj, "A robust repetitive-control design for a class of uncertain stochastic dynamical systems," *IEEE Trans. Circuits Syst. II*, vol. 64, no. 4, pp. 427–431, Apr. 2017.
[27] S. Yang, P. Wang, Y. Tang, and L. Zhang, "Explicit phase lead filter design in repetitive control for voltage harmonic mitigation of vsi-based islanded microgrids," *IEEE Trans. Ind. Electron.*, vol. 64, no. 1, pp. 817–826, Jan. 2017.
[28] H. Muramatsu and S. Katsura, "An adaptive periodic-disturbance observer for periodic-disturbance suppression," *IEEE Trans. Ind. Informat.*, vol. 14, no. 10, pp. 4446–4456, Oct. 2018.
[29] S. Bittanti and P. Colaneri, "Invariant representations of discrete-time periodic systems," *Automatica*, vol. 36, no. 12, pp. 1777–1793, Dec. 2000.
[30] P. Zhang, S. X. Ding, and P. Liu, "A lifting based approach to observer based fault detection of linear periodic systems," *IEEE Trans. Autom. Control*, vol. 57, no. 2, pp. 457–462, Feb. 2012.
[31] I. Markovsky, J. Goos, K. Usevich, and R. Pintelon, "Realization and identification of autonomous linear periodically time-varying systems," *Automatica*, vol. 50, no. 6, pp. 1632–1640, Jun. 2014.
[32] E. Sariyildiz and K. Ohnishi, "Stability and robustness of disturbance-observer-based motion control systems," *IEEE Trans. Ind. Electron.*, vol. 62, no. 1, pp. 414–422, Jan. 2015.
[33] W. H. Chen, J. Yang, L. Guo, and S. Li, "Disturbance-observer-based control and related methods—An overview," *IEEE Trans. Ind. Electron.*, vol. 63, no. 2, pp. 1083–1095, Feb. 2016.
[34] S. Jafari and P. A. Ioannou, "Rejection of unknown periodic disturbances for continuous-time MIMO systems with dynamic uncertainties," *Int. J. Adapt. Control Signal Process.*, vol. 30, no. 12, pp. 1674–1688, Dec. 2016.
[35] I. D. Landau, A. C. Silva, T.-B. Airimitoaie, G. Buche, and M. Noë, "Benchmark on adaptive regulation-rejection of unknown/time-varying multiple narrow band disturbances," *Eur. J. Control*, vol. 19, no. 4, pp. 237–252, Jul. 2013.
[36] I. D. Landau, M. Alma, A. Constantinescu, J. J. Martinez, and M. Noë, "Adaptive regulation-rejection of unknown multiple narrow band disturbances (a review on algorithms and applications)," *Control Eng. Pract.*, vol. 19, no. 10, pp. 1168–1181, Oct. 2011.
[37] R. Marino and P. Tomei, "Adaptive notch filters are local adaptive observers," *Int. J. Adapt. Control Signal Process.*, vol. 30, no. 1, pp. 128–146, Jan. 2016.
[38] M. Mojiri and A. R. Bakhshai, "An adaptive notch filter for frequency estimation of a periodic signal," *IEEE Trans. Autom. Control*, vol. 49, no. 2, pp. 314–318, Feb. 2004.
[39] B. K. Kim and W. K. Chung, "Advanced disturbance observer design for mechanical positioning systems," *IEEE Trans. Ind. Electron.*, vol. 50, no. 6, pp. 1207–1216, Dec. 2003.
[40] J. N. Yun and J. B. Su, "Design of a disturbance observer for a two-link manipulator with flexible joints," *IEEE Trans. Control Syst. Technol.*, vol. 22, no. 2, pp. 809–815, Mar. 2014.
[41] H. Grabner, W. Amrhein, S. Silber, and W. Gruber, "Nonlinear feedback control of a bearingless brushless DC motor," *IEEE/ASME Trans. Mechatronics*, vol. 15, no. 1, pp. 40–47, Feb. 2010.
[42] C. Lascu, S. Jafarzadeh, M. S. Fadali, and F. Blaabjerg, "Direct torque control with feedback linearization for induction motor drives," *IEEE Trans. Power Electron.*, vol. 32, no. 3, pp. 2072–2080, Mar. 2017.
[43] M. Ruderman, "Tracking control of motor drives using feedforward friction observer," *IEEE Trans. Ind. Electron.*, vol. 61, no. 7, pp. 3727–3735, Jul. 2014.
[44] M. Ruderman and M. Iwasaki, "Observer of nonlinear friction dynamics for motion control," *IEEE Trans. Ind. Electron.*, vol. 62, no. 9, pp. 5941–5949, Sep. 2015.
[45] T. Murakami, F. Yu, and K. Ohnishi, "Torque sensorless control in multidegree-of-freedom manipulator," *IEEE Trans. Ind. Electron.*, vol. 40, no. 2, pp. 259–265, Apr. 1993.
[46] S. Katsura, Y. Matsumoto, and K. Ohnishi, "Modeling of force sensing and validation of disturbance observer for force control," *IEEE Trans. Ind. Electron.*, vol. 54, no. 1, pp. 530–538, Feb. 2007.

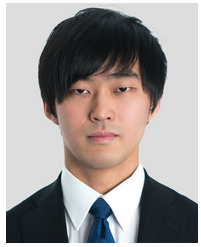

Hisayoshi Muramatsu (S'16) received the B.E. degree in system design engineering and the M.E. degree in integrated design engineering, in 2016 from Keio University, Yokohama, Japan, where he is currently working toward the Ph.D. degree in integrated design engineering.

Since 2019, he has been a Research Fellow with the Japan Society for the Promotion of Science. His research interests include control engineering, motion control, and mechatronics.

Seiichiro Katsura (S'03–M'04) received the B.E. degree in system design engineering and the M.E. and Ph.D. degrees in integrated design engineering from Keio University, Yokohama, Japan, in 2001, 2002, and 2004, respectively.

From 2003 to 2005, he was a Research Fellow with the Japan Society for the Promotion of Science (JSPS). From 2005 to 2008, he was with the Nagaoka University of Technology, Nagaoka, Japan. Since 2008, he has been with the Department of System Design Engineering, Keio University, Yokohama, Japan. He is currently working as a Professor with Department of System Design Engineering, Keio University. In 2017, he was a Visiting Researcher with the Laboratory for Machine Tools and Production Engineering of RWTH Aachen University, Aachen, Germany. His research interests include applied abstraction, human support, data robotics, wave system, systems energy conversion, and electromechanical integration systems.

Prof. Katsura serves as an Associate Editor of the IEEE TRANSACTIONS ON INDUSTRIAL ELECTRONICS and Technical Editor of the IEEE/ASME TRANSACTIONS ON MECHATRONICS. He was the recipient of The Institute of Electrical Engineers of Japan Distinguished Paper Awards in 2003 and 2017, IEEE Industrial Electronics Society Best Conference Paper Award in 2012, and JSPS Prize in 2016.